AGU PUBLICATIONS

Geophysical Research Letters

RESEARCH LETTER
10.1002/2014GL060517

Key Points:
- Amplitude of the M2 can vary by 8–10% and the M4 amplitude by 12–30%
- Annual phase variations of M2 and M4 are in the range of 3–15°
- Residual sediment transport can vary by 10–50%

Correspondence to:
U. Gräwe,
ulf.graewe@io-warnemuende.de

Citation:
Gräwe, U., H. Burchard, M. Müller, and H. M. Schuttelaars (2014), Seasonal variability in M_2 and M_4 tidal constituents and its implications for the coastal residual sediment transport, *Geophys. Res. Lett.*, *41*, 5563–5570, doi:10.1002/2014GL060517.

Received 12 MAY 2014
Accepted 18 JUL 2014
Accepted article online 24 JUL 2014
Published online 4 AUG 2014

Seasonal variability in M_2 and M_4 tidal constituents and its implications for the coastal residual sediment transport

Ulf Gräwe[1], Hans Burchard[1], Malte Müller[2], and Henk M. Schuttelaars[3]

[1]Department of Physical Oceanography and Instrumentation, Leibniz Institute for Baltic Sea Research, Rostock, Germany, [2]Research and Development Department, Norwegian Meteorological Institute, Oslo, Norway, [3]Delft Institute of Applied Mathematics, Delft University of Technology, Delft, Netherlands

Abstract We use an observational data set of tidal gauges in the North Sea to investigate the annual cycle of the M_2 and M_4 amplitudes and phases. The sea surface elevation amplitude of the M_2 can vary by 8–10% and the M_4 amplitude by 12–30% over the course of the year, with larger amplitudes in summer. The annual phase variations are in the range of 3–15°. The reason for these variations is the thermal structure of the North Sea: a well-developed thermocline in summer and well-mixed water column during winter. The interaction of the M_2 and M_4 tides is one of the main drivers of the residual sediment transport. Using an analytical model, the seasonal variability in residual sediment transport is estimated. This transport can vary by 10–50% over the course of the year. These variations are mainly related to the seasonal variability of the M_2 and M_4 amplitudes.

1. Introduction

The effect of seasonal variation in the major tidal constituent M_2 has received considerable attention. For example, the Northwest European Shelf is one of the most intensively surveyed shelves in the world with over 200 coastal and pelagic tidal gauges. Furthermore, the midlatitude location of the North Sea favors the usage of TOPEX/POSEIDON satellite data. *Huess and Andersen* [2001] used these data to investigate the sea surface elevation (SSE) of the shallow water tides on the shelf. They estimate an annual variation of the M_2 amplitude of less than 5%. *Leeuwenburgh et al.* [1999] and *Andersen* [1999] investigated the seasonality of the M_2 SSE by using a combination of satellite observations and tidal gauges. They could show that the amplitude can vary by 10% over the course of the year. However, an estimation of the significance levels or even a detailed explanation was missing. Moreover, neither *Huess and Andersen* [2001] nor *Leeuwenburgh et al.* [1999] and *Andersen* [1999] gave an estimation of the seasonality of the M_2 SSE phase. A seasonality of 4–8% in the M_2 tidal SSE was reported for the Yellow Sea [*Kang et al.*, 1995], and a variation of 6% for Victoria, Canada [*Foreman et al.*, 1995].

With the help of analytical and simplified numerical models, *Müller* [2012] shows that the seasonal thermal stratification in the North Sea is the main driver of the seasonal variation in the SSE amplitude of the major tidal constituent M_2. The summer two-layer system leads to a reduction in energy loss of the propagating tidal wave, giving higher tidal amplitudes in summer. The same mechanism for seasonal tides can be found in other coastal ocean regions, as shown by *Müller et al.* [2014] with a global high-resolution ocean circulation and tide model approach.

Since the overtides result from the interaction of the M_2 tidal constituent with itself or external forcing, it is to be expected that the seasonal cycle of the M_2 affects the overtides (M_4, M_6, M_8, ...). Previous research focused on the M_2 amplitude of the SSE without considering the seasonality of other tidal constituents and their phases. *Van de Kreeke and Robaczewska* [1993] and *Hoitink et al.* [2003] showed that the M_2 and its overtides M_4 and M_6 are dominating the residual suspended particulate matter (SPM) transport in the Wadden Sea, the southeastern part of the North Sea. Moreover, *Burchard et al.* [2013] show in idealized numerical studies that the suspended load can be dominated by the asymmetric bottom shear stress, caused by the M_2 and M_4 amplitude phase differences. Especially in the Wadden Sea, with its large intertidal flats and shallow regions, which promote nonlinear tidal interaction, seasonality in the residual SPM transport can be expected.

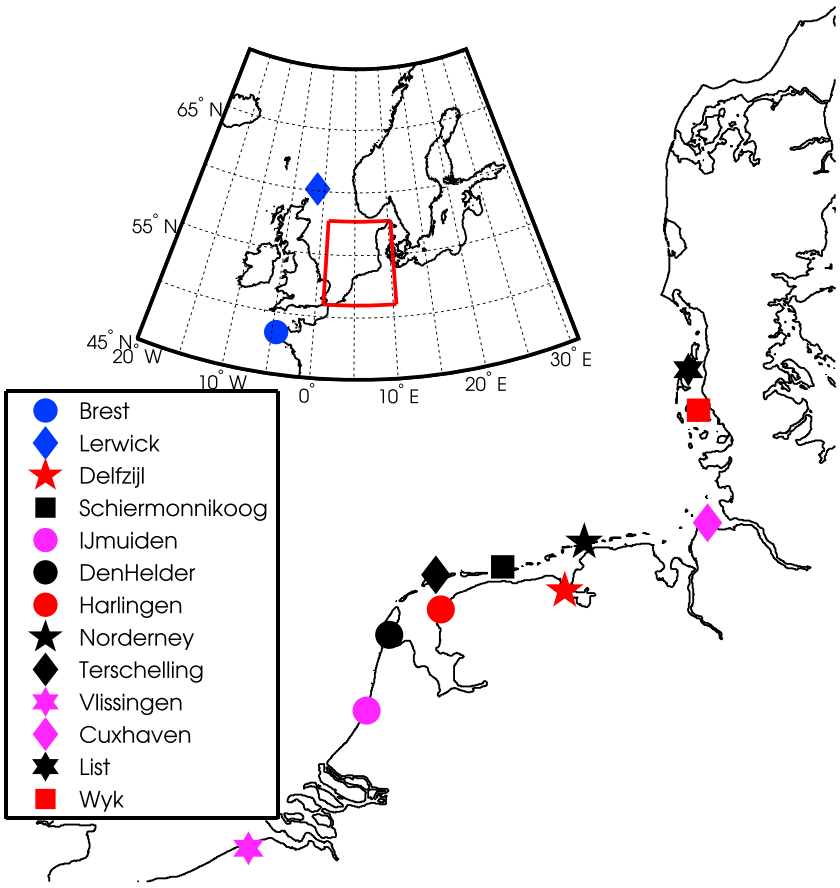

Figure 1. Map of the Wadden Sea and location of the used tidal gauges. The inset shows a map of the Northwest European Shelf and the location of the Wadden Sea.

The first aim of this paper is to investigate the seasonal variability in M_2 and M_4 SSE amplitudes and phases by analyzing tidal gauge data from several stations on the Northwest European Shelf and in the Wadden Sea (Figure 1). In view of this, our second aim is to investigate the seasonality of the residual coastal sediment transport in the Wadden Sea by using a simplified analytical model. Finally, we use recent measurements of the SPM transport in the Dutch Wadden Sea [*Nauw et al.*, 2014] to show that our bulk estimates are consistent with the measured fluxes.

2. Methods and Data

2.1. Observational Data

Tidal gauge observations were collected from 13 stations at the European Shelf, in the North Sea, and the Wadden Sea (see Figure 1). All records span at least 18 successive years, with most stations having an observational record of 30 years (Table 1). An exception is Cuxhaven with data coverage from 1917 to 2012. Note that during the last century, the Wadden Sea experienced significant man-made changes. The construction of the Afsluitdijk (a dam separating the Wadden Sea from the Lake IJssel, completed in 1932), the formation of the Lauwersmeer in 1969, and the land reclamation in Meldorf Bay in 1978 have influenced the tidal signal in the Wadden Sea. Thus, the past and ongoing changes will also affect the tidal signal. However, since the annual cycle is a periodic signal, we can safely separate it from the long-term changes.

To distinguish between large-scale forcing and local effects, we grouped the gauge station into four classes (see fourth column in Table 1). The stations Brest and Lerwick are regarded as open water stations and only see the incoming tidal wave from the open ocean (*OW*). Furthermore, we use the class "coastal water" (*CW*), which is characterized by a straight coastline, and the location of the gauge is not in the vicinity of an inlet. The third class consists of gauge stations directly located in tidal inlets (*TI*). The final class groups stations

Table 1. Data Coverage, Sampling Interval, and Type of the Gauge Stations[a]

Station	Coverage	Sampling Interval	Type	*L*	*H*
Brest	1980–2009	60 min	OW	-	-
Lerwick	1980–2010	60 min	OW	-	-
Delfzijl	1980–1990	60 min	TF	80 km	12 m
	1991–2010	10 min			
Schiermonnikoog	1980–1990	60 min	TI	20 km	10 m
	1991–2010	10 min			
IJmuiden	1980–1990	60 min	CW	∞	15 m
	1991–2010	10 min			
Den Helder	1980–1990	60 min	TI	30 km	15 m
	1991–2010	10 min			
Harlingen	1980–1990	60 min	TF	30 km	6 m
	1991–2010	10 min			
Terschelling	1980–1990	60 min	TI	12 km	10 m
	1991–2010	10 min			
Vlissingen	1980–1990	60 min	CW	∞	20 m
	1991–2010	10 min			
Cuxhaven	1917–1987	60 min	CW/TI	120 km	16 m
	1997–2010	20 min			
Norderney	1996–2013	10 min	TI	20 km	8 m
List	1995–2013	10 min	TI	20 km	10 m
Wyk	1995–2013	10 min	TF	22 km	6 m

[a]OW, open water; CW, coastal water; TI, tidal inlet; and TF, tidal flat. The two last columns indicate the channel length and average water depth at the stations.

that are surrounded by large tidal flat areas (*TF*). In the following figures, we use a unique color coding for these four classes: blue for OW, magenta for CW, black for TI, and red for TF stations.

2.2. Data Analysis

In order to investigate the temporal variation of the amplitudes and the phases of the tidal constituents, we use the MATLAB-package T-TIDE [*Pawlowicz et al.*, 2002] to analyze the observed time series. Besides the information about the amplitude and phase of the M_2 and M_4 tidal constituents, T-TIDE also provides confidence intervals for the estimated parameters. The computation of the 95% confidence intervals is based on the assumption that the errors follow a Gaussian white noise process. Since we are interested in variations of the tidal constituents on an intra-annual scale, we split each year into several smaller intervals. We followed the suggestions of *Leeuwenburgh et al.* [1999] and *Huess and Andersen* [2001] and used a window length of 3 months. A sensitivity analysis with varying window lengths indicated that this was a trade-off between narrow 95% confidence intervals (longer window) and a representative resolution of the annual cycle (shorter window). By shifting the window 5 days each time, a description of the variation of the tides over the individual years was found. To remove secular trends [*Woodworth et al.*, 2007; *Müller et al.*, 2011], the time series of monthly mean amplitudes were detrended. Furthermore, we removed long-term oscillations by using a forced fit to the nodal cycle (T=18.6 years). Afterward, we constructed the seasonal cycle of amplitude and phase for the individual tidal constituents.

3. Seasonal Variations in Tidal Signal

The M_2 and M_4 tides are changing on seasonal, annual, and on secular time scales (Figures 2a and 2b for station Cuxhaven). The data clearly show that the seasonal cycle of the M_2 and M_4 amplitudes is a persistent feature over the last century. The summer amplitudes are for all record years larger than the winter amplitudes. The seasonal changes of the M_2 tide amplitude are well explained by changes in thermal stratification [*Müller*, 2012; *Müller et al.*, 2014]. Besides the linear secular trends [*Woodworth et al.*, 2007; *Müller et al.*, 2011], a longer period variability with a time scale of approximately 50 years is visible. However, these long-term changes are not well understood, so far [*Müller et al.*, 2011]. If we assume that the M_4 tide is mainly generated locally, we would expect that the ratio of $\left(a_{M_2}\right)^2 / a_{M_4}$ is constant and that the M_4 interannual and secular changes mimic that of the M_2 tide. However, Figure 2c indicates that the generation of the M_4 tide

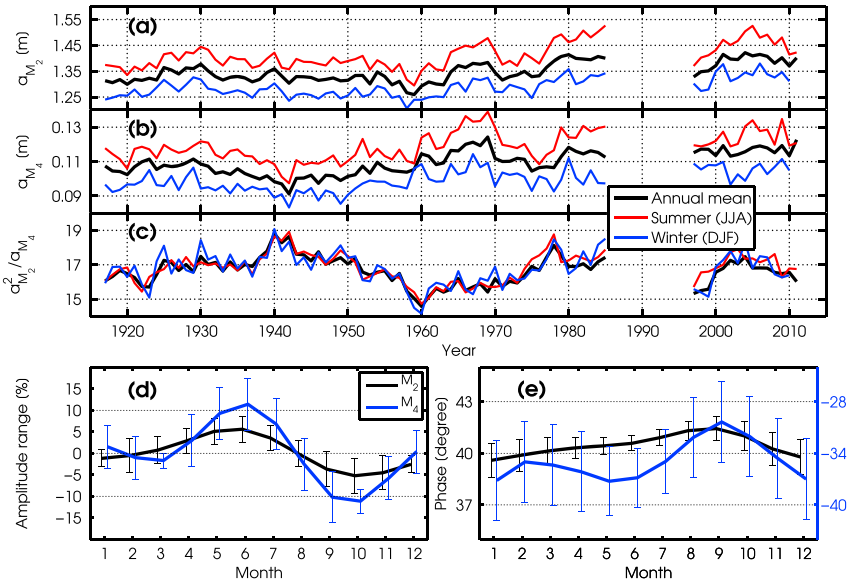

Figure 2. Analysis of tide gauge data for Cuxhaven: (a) time series of the M_2 amplitude (a_{M_2}) annual mean, summer (June-July-August (JJA)) and winter (December-January-February (DJF)) amplitude, (b) time series of M_4 amplitude (a_{M_4}) annual mean, summer (JJA) and winter (DJF) amplitude, and (c) ratio of $\left(a_{M_2}\right)^2$ and a_{M_4}. (d) The annual cycle of amplitude range and (e) annual cycle of phase variation. Vertical bars indicate the 95% confidence intervals. Note that only for this plot the tidal analysis is done for the period 1917–2012. Moreover, no detrending was applied.

is more complex, presumably induced by variations at nonlocal generation sites which indeed can be thousands of kilometers distant [*Ray*, 2007]. On annual time scales, the ratio $\left(a_{M_2}\right)^2 / a_{M_4}$ is constant for summer and winter season.

In Figures 2d and 2e we show the resulting annual cycle (for the period 1917–2010) for the M_2 and M_4 amplitudes and phases at Cuxhaven. The amplitudes are largest in July and are lowest in September/October at the time of the breakdown of the thermal stratification in the central North Sea. The occurrences of the lowest amplitudes coincide with the largest SSE phase values. The relative phase difference ($2\phi_{a_{M_2}} - \phi_{a_{M_4}}$) [*Hoitink et al.*, 2003] is well correlated with the annual cycle of the M_2 amplitude (not shown), largest values during July (118°) and lowest values during September/October (113°).

The annual variations of the M_2 tide, Figure 3a indicates that the SSE amplitude can vary between 6 and 11%, of the annual mean amplitude, for the shallow water stations. The SSE phase can vary by 2 to 6°. Additionally, a clear grouping of the stations is visible. The open ocean stations show the smallest variations, whereas the largest seasonal range is found for the tidal flat stations. Note that the seasonal variations at all stations are significant (except for Lerwick).

A similar behavior can be seen for the M_4 tide (Figure 3b). Again, the tidal flat stations show the largest variations in tidal amplitude (25–30%) and phase (10–15%). A comparable clustering of the different station classes is visible. Figure 3b also indicates that the confidence intervals are larger than for the M_2. However, the seasonal variability is still significant.

Figure 3 also shows that the incoming oceanic tidal wave (Brest, Lerwick) has only little annual variations. The seasonal cycle is only generated within the North Sea, where the water motion is strongly affected by the thermal stratification in the central North Sea [*Müller*, 2012].

4. Impact on Residual SPM Transport

The estimation of possible consequences of the seasonality of the M_2 and M_4 tidal signal is motivated by the findings of *Van de Kreeke and Robaczewska* [1993], who indicate that the M_2 constituent and its overtides are the major contributions to the tidally averaged mass transport. Moreover, the M_2 and M_4 velocity relative

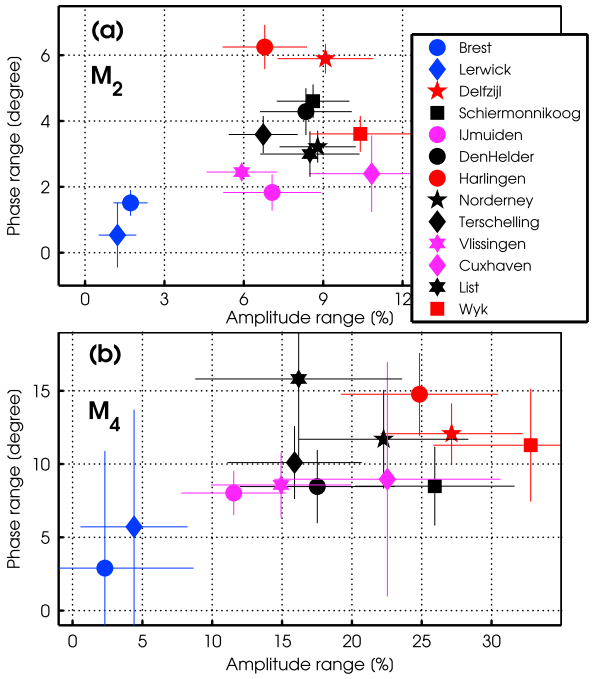

Figure 3. Annual range in tidal amplitude and phase for (a) M_2 and (b) M_4. Thin lines indicate the 95% confidence intervals.

phase differences trigger the asymmetry of the bottom shear, which can be a dominating factor in the total sediment flux [*Burchard et al.*, 2013].

To get a rough estimate of the expected tidal residual sediment transport, we first reconstructed the sea surface elevation $\eta(t)$ based on the M_2 and M_4 constituents:

$$\eta(t) = a_{M_2}\cos\left(\omega_{M_2}t - \phi_{M_2}\right) + a_{M_4}\cos\left(\omega_{M_4}t - \phi_{M_4}\right), \quad (1)$$

where a, ω, and ϕ represent the SSE amplitude, the frequency, and phase of the individual tidal constituent.

Van de Kreeke and Robaczewska [1993] and *Hoitink et al.* [2003] used the above expression to convert the time series of sea surface elevation into a time series of depth-averaged velocities based on shallow water wave theory [*Craik*, 2004] for a fully propagating tidal wave. However, in the Wadden Sea or any other semienclosed water body, the tidal wave in an estuary is composed of an incoming wave and an outgoing reflected wave whose amplitude is reduced by friction. The outgoing wave is caused by the reflection at the landward end of the basin. The resulting standing wave can be additionally modified by possible resonance conditions. To account for this in the computation of the velocities at the gauge stations, we solved the linearized mass balance and momentum balance equations for a simple rectangular channel with uniform depth [*Ippen*, 1966]:

$$\partial_t\eta + H\partial_x U = 0$$
$$\partial_t U + g\partial_x\eta + K\,U = 0, \quad (2)$$

with the depth-averaged current U, the linear friction coefficient K, and g the earth acceleration. The channel has a length L, and a no flux boundary condition is imposed at the end of the channel at $x = L$. A detailed derivation and the analytical solution can be found in *Ippen* [1966] or *Officer* [1976]. Input parameters are a_{M_2}, a_{M_4}, ϕ_{M_2}, and ϕ_{M_4} at $x = 0$, the estimated channel length L, the averaged water depth H, and the friction coefficient K. Reasonable values for L and H are given in Table 1 and are estimated from bathymetric maps. Note that for the stations Harlingen, Delfzijl, and Wyk, the distance from the inlet was taken into account. For the friction coefficient we used $K = 2.5 \cdot 10^{-3}\ s^{-1}$.

Using these estimates of U_{M_2}, U_{M_4}, $\phi_{U_{M_2}}$, and $\phi_{U_{M_4}}$ (based on the solution of equation (2)), we can estimate the residual sediment transport. Here we follow the work of *Bagnold* [1966] who developed a theory based on an energy concept. *Bagnold* [1966] relates the bed load transport rate Q_B to the work done by the fluid. In this approach the transport due to the tidal motion is proportional to U^3. *Groen* [1967] developed a simple mathematical framework to include also suspended load (Q_S). Although Groen's model takes into account settling lag effects of SPM, in the following, we assume that the total transport (total load) $Q = Q_B + Q_S$ of material instantaneously reacts on changes in $U(t)$. The residual transport is then proportional to the average of U^3 over a tidal period. This can formally be calculated from

$$\langle Q\rangle = \langle Q_B\rangle + \langle Q_S\rangle \propto \frac{1}{T}\int_0^T U(t)^3\mathrm{d}t = \langle U^3\rangle. \quad (3)$$

Here $\langle\cdot\rangle$ indicates the average over the M_2 tidal period T. Integrating the above equation reduced the expression for the residual transport to

$$\langle Q\rangle \propto \frac{3}{4}{U_{M_2}}^2 U_{M_4}\cos\left(2\phi_{U_{M_2}} - \phi_{U_{M_4}}\right). \quad (4)$$

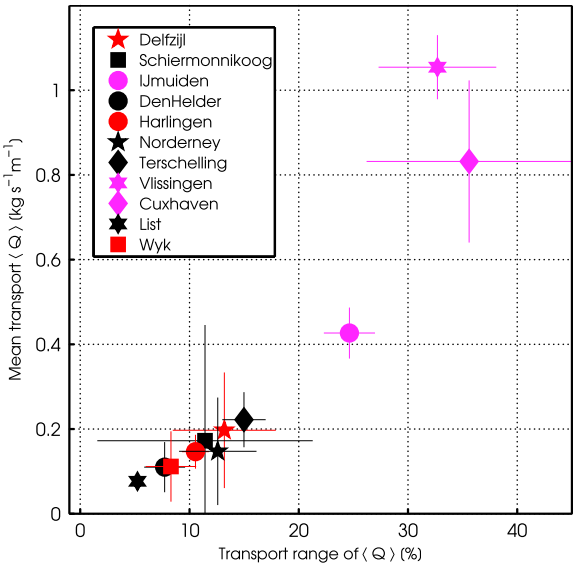

Figure 4. Estimated mean depth-integrated sediment transport and annual sediment transport range. Thin lines indicate the 95% confidence intervals.

Equation (4) indicates that the amplitudes and the relative phase differences are important in determining the magnitude of the residual sediment transport. The direction of the residual transport can change sign for different relative phases. To compute the total transport $\langle Q \rangle$ we have to find the proportionality factor. At first, assume that

$$\langle Q \rangle = \langle U\, C \rangle, \tag{5}$$

with the depth-averaged SPM concentration C and an approximate, instantaneous balance between erosion αU^2 and deposition γC [*van Rijn*, 1993]:

$$\partial_t C = 0 = \alpha U^2 - \gamma C. \tag{6}$$

The parameter α is related to the SPM properties, with typical values of α of $O(10^{-2}–10^{-4}$ kgsm$^{-4})$ as reported by *Fredsøe and Deigaard* [1992]. The parameter γ is related to the settling velocity w_s and the vertical diffusion coefficient κ_V. Assuming a constant κ_V, it follows from *van Rijn* [1993] that $\gamma = w_s^2/\kappa_V$. Inserting into equation (5) yields

$$\langle Q \rangle = \langle U\, U^2\, \frac{\alpha}{\gamma} \rangle = \frac{\alpha}{\gamma} \langle U^3 \rangle. \tag{7}$$

If we assign typical values of $\alpha = 10^{-3}$ kgsm^{-4}, $w_s = 0.001$ m/s, and $\kappa_V = 0.01$ m^2/s [*Burchard et al.*, 2013], α/γ takes values of 10 kg s^{-2} m^{-4}. Equation (7) is now an expression for the depth-integrated residual transport per unit width.

In Figure 4 we plotted the average total sediment transport per unit width (equation (7)) and the annual transport variability (measured by the difference between the annual maximum transport and the annual minimum transport value). The results indicate that for all stations a significant seasonal cycle in residual transport exists. These seasonal variations are most pronounced for the coastal stations IJmuiden, Vlissingen, and Cuxhaven. The residual transport can vary by 40% over the course of the year. Additionally, the annual transport for these three stations is largest. A possible explanation is that the tidal wave along the open coast is mostly a propagating one. For stations like Wyk6 or Harlingen, which are deep inside the tidal flat regions, the tidal wave has the character of a standing wave. Thus, the total annual transport is significantly reduced. However, the tidal flat stations still show an annual transport range of 6 to 12%.

To estimate the uncertainty caused by the estimates of L, H (Table 1), and K, we varied the parameters by 10%. The analysis showed that the friction parameter has the smallest impact. This can be attributed to the fact that all tidal basins are short. Thus, frictional damping is of minor importance. The resulting variations in mean transport and range are for all stations within the 95% confidence intervals and therefore not individually shown. It can thus be concluded that the mean transport and the annual range show significant variations over the course of the year.

To verify our estimations, we use the long-term observations of the suspended sediment fluxes through the Marsdiep [*Nauw et al.*, 2014], the tidal inlet at Den Helder. They used the backscatter signal of a ferry mounted acoustic Doppler current profiler and the measured velocity profiles to estimate the SPM transport through the inlet. The ferry crosses the Marsdiep every 30 min during regular working hours. Although the measurements poses a challenging task to analyze, the resulting data set gives a good estimate of the SPM fluxes for the period 2003–2005. Assuming a channel width of 3000 m and a mean depth-integrated transport $\langle Q \rangle = 0.17$ kg s^{-1} m^{-1} (Figure 4) results in a channel-integrated transport of 500 kg/s. This is in the right order of magnitude than the estimates of *Nauw et al.* [2014], who quantified the residual SPM transport as 230–360 kg/s (for period 2003–2005). Moreover, the observations and our estimates show an inward

Table 2. Explained Variance in Annual SPM Transport Range for the Individual Contribution of SSE Amplitudes and Phases of M_2 and M_4 [a]

Parameter	a_{M_2}	ϕ_{M_2}	a_{M_4}	ϕ_{M_4}
Delfzijl	33	9	49	9
Schiermonnikoog	39	1	59	1
IJmuiden	51	2	41	6
DenHelder	40	11	39	10
Harlingen	6	38	11	45
Terschelling	29	15	35	21
Vlissingen	44	0	55	1
Cuxhaven	26	16	27	31
Norderney	36	5	53	6
List	34	3	55	8
Wyk	32	7	50	11

[a]Values are given in percent of the total annual variation.

directed transport of sediment. This also means that for Den Helder/Marsdiep the annual variability of 8% (Figure 4) translates to a 10–20 kg/s variation of residual SPM flux over the course of the year.

5. Driver of Residual Transport Variability

To identify the major driver of the residual transport, we computed the contribution of SSE amplitude and phase of M_2 and M_4 to the total seasonal variation. In Table 2, the explained variance in annual transport range is presented. For most of the stations, the interaction of the M_2 and M_4 amplitudes dominates the seasonal signal. Even for stations like Schiermonnikoog, Norderney, or List, the annual variations in the M_4 amplitude explain more than 50% of the total signal. This is remarkable, since the residual transport has a linear dependency on the M_4 amplitude but a quadratic one on the M_2 amplitude (equation (4)). Although the importance of the phase differences is small for most of the stations, for stations like Harlingen or Cuxhaven, they can explain more than 50% of the total variations.

6. Summary

In the Wadden Sea several drivers of seasonal variability exist. Besides the seasonal cycle in storm activity, temperature, river runoff, and biological activity, we identify a new contributor. The M_2 and M_4 amplitudes and phases show a pronounced seasonal variation. Due to the interaction of M_2 and M_4 amplitudes and phases, a seasonal signal in the residual sediment transport is induced. By using an analytical model to convert the time series of sea surface elevation into depth-averaged velocities, we separated the tidal wave into a propagating and standing wave part. This gave a more reliable estimate of the residual velocities at the gauge stations. However, for some of the stations like Cuxhaven and Vlissingen, local baroclinic effects cannot be ruled out due to high river discharge (Elbe and Rhine). Nevertheless, our idealized analytical model enabled us to estimate the annual variation in the sediment flux. The annual variations in mass flux vary by 10–50% over the course of the year. These variations are related to the seasonal variability of the M_2 and M_4 SSE amplitudes. Only for a limited number of stations, the seasonal variations in the residual transport are dominated by the annual variability of the M_2 and M_4 SSE phases.

As already discussed, the Yellow Sea [*Kang et al.*, 1995] and the Korean Sea show similar characteristics in the seasonality of the M_2 amplitude and phase as the North Sea. Since the Korean Sea also shows large tidal flat regions, the same analysis could be applied.

At present, the annual cycle of the M_2 and M_4 interaction poses a challenge to numerical models. Since the seasonal cycle in the tidal signal is largely a baroclinic (thermal) process [*Müller*, 2012], vertically averaged numerical transport models do not capture this effect. The same holds for models that underestimate the vertical stratification in the central North Sea. This directly implies that an important driver is missing which modulates the residual sediment transport, as shown by our data analysis.

Acknowledgments
The German Federal Maritime and Hydrographic Agency, Rijkswaterstraat, Permanent Service for Mean Sea Level, and Ministry of Energy, Agriculture, the Environment and Rural Areas Schleswig-Holstein kindly provided gauge data. This work was supported by the German Federal Ministry of Research and Education in the framework of the project PACE (The future of the Wadden Sea sediment fluxes: still keeping pace with sea level rise?, FKZ 03F0634A) and the project SH-Trend (simulation of the long-term morphological trends in tidal systems of the west coast of Schleswig-Holstein), funded by the Ministry of Energy, Agriculture, the Environment and Rural Areas of Schleswig-Holstein.

The Editor thanks two anonymous reviewers for their assistance in evaluating this paper.

References

Andersen, O. B. (1999), Shallow water tides in the northwest European shelf region from TOPEX/POSEIDON altimetry, *J. Geophys. Res.*, *104*, 7729–7741.

Bagnold, R. A. (1966), An approach to the sediment transport problem from general physics, *PUSGS Professional Paper: 422-I*, pp. I1-I37, U.S. Govt. Print. Off., Washington, D. C.

Burchard, H., H. M. Schuttelaars, and W. R. Geyer (2013), Residual sediment fluxes in weakly-to-periodically stratified estuaries and tidal inlets, *J. Phys. Oceanogr.*, *43*, 1841–1861.

Craik, A. D. (2004), The origins of water wave theory, *Annu. Rev. Fluid Mech.*, *36*, 1–28.

Foreman, M. G. G., R. A. Walters, R. F. Henry, C. P. Keller, and A. G. Dolling (1995), A tidal model for eastern Juan de Fuca Strait and the southern Strait of Georgia, *J. Geophys. Res.*, *100*(C1), 721–740.

Fredsøe, J., and R. Deigaard (1992), *Mechanics of Coastal Sediment Transport*, World Scientific, Singapore.

Groen, P. (1967), On the residual transport of suspended matter by an alternating tidal current, *Neth. J. Sea Res.*, *3*, 564–574.

Hoitink, A. J. F., P. Hoekstra, and D. S. van Maren (2003), Flow asymmetry associated with astronomical tides: Implications for the residual transport of sediment, *J. Geophys. Res.*, *108*(C10), 3315, doi:10.1029/2002JC001539.

Huess, V., and O. B. Andersen (2001), Seasonal variation in the main tidal constituent from altimetry, *Geophys. Res. Lett.*, *28*, 567–570.

Ippen, A. T. (1966), Tidal dynamics in estuaries, Part I: Estuaries of rectangular cross-section, in *Estuary and Coastline Hydrodynamics*, edited by A. T. Ippen et al., pp. 493–522, McGraw-Hill, New York.

Kang, S. K., J. Chung, S.-R. Lee, and K.-D. Yum (1995), Seasonal variability of the M_2 tide in the seas adjacent to Korea, *Cont. Shelf Res.*, *15*, 1087–1113.

Leeuwenburgh, O., O. Andersen, and V. Huess (1999), Seasonal tide variations from tide gauges and altimetry, *Phys. Chem. Earth Part A*, *24*, 403–406.

Müller, M. (2012), The influence of changing stratification conditions on barotropic tidal transport and its implications for seasonal and secular changes of tides, *Cont. Shelf Res.*, *47*, 107–118.

Müller, M., B. K. Arbic, and J. X. Mitrovica (2011), Secular trends in ocean tides: Observations and model results, *J. Geophys. Res.*, *116*, C05013, doi:10.1029/2010JC006387.

Müller, M., J. Y. Cherniawsky, M. G. G. Foreman, and J.-S. von Storch (2014), Seasonal variation of the M_2 tide, *Ocean Dyn.*, *64*, 159–177.

Nauw, J., L. Merckelbach, H. Ridderinkhof, and H. van Aken (2014), Long-term ferry-based observations of the suspended sediment fluxes through the Marsdiep inlet using acoustic Doppler current profilers, *J. Sea Res.*, *87*, 17–29.

Officer, C. B. (1976), *Physical Oceanography of Estuaries (and Associated Coastal Waters)*, Wiley, New York.

Pawlowicz, R., B. Beardsley, and S. Lentz (2002), Classical tidal harmonic analysis including error estimates in MATLAB using T_TIDE, *Comput. Geosci.*, *28*, 929–937.

Ray, R. D. (2007), Propagation of the overtide M_4 through the deep Atlantic Ocean, *Geophys. Res. Lett.*, *34*, L21602, doi:10.1029/2007GL031618.

Van de Kreeke, J., and K. Robaczewska (1993), Tide-induced residual transport of coarse sediment; application to the EMS estuary, *Neth. J. Sea Res.*, *31*, 209–220.

van Rijn, L. C. (1993), *Principles of Sediment Transport in Rivers, Estuaries and Coastal Seas, Part 1*, Aqua Publications, The Netherlands.

Woodworth, P. L., S. M. Shaw, and D. L. Blackman (2007), Secular trends in mean tidal range around the British Isles and along the adjacent European coastline, *Geophys. J. Int.*, *104*, 593–609.